21st Australasian Fluid Mechanics Conference
Adelaide, Australia
10-13 December 2018

Modes of Synchronisation for Oscillatory Cylinder in Steady Flow at Various Angles of Attack

F. Tong[1], L. Cheng[1,2], H. An[1] and H. Jiang[1]

[1]Department of Civil, Environmental and Mining Engineering
The University of Western Australia, Crawley, WA, 6009, Australia

[2]DUT-UWA Joint Research Centre, State Key Laboratory of Coastal and Offshore Engineering
Dalian University of Technology, Dalian, 116024, China

Abstract

We present a study on the flow around a circular cylinder under controlled oscillation in steady current at a low Reynolds number of 100. Three different angles of attack between the direction of the motion and the far-field flow have been investigated at different oscillation frequencies. The focus of the present report is on the frequency responses of the hydrodynamic forces and the modes of wake formation. It shows that the inclined oscillation, where the motion intersect the freestream at a 45°, leads to substantial changes to hydrodynamic forces from those of the in-line (0°) or transverse (90°) oscillations. These changes are demonstrated to be related to the flow synchronisation phenomenon between the vortex shedding and cylinder motion, which is found in a wide range of oscillation frequencies for the inclined oscillation.

Introduction

A circular cylinder subject to forced oscillation in steady current exhibits a range of rich flow phenomena due to the self-excited wake instability and the externally posed perturbation [5, 6, 9, among others]. At certain combinations of driving frequency (f_d) and amplitude (A) of oscillations, vortex shedding may synchronise with cylinder oscillation, where the flow is characterised by ordered and repeatable wake formation. Such a feature can be used in active wake control and many studies were devoted to the wake flows by moving a circular cylinder either transversely or in-line to the direction of the incoming flow [1, 3, 6, etc.].

Among these efforts, Williamson and Roshko [11] reported a series of distinct flow regimes for a transversely oscillatory cylinder, identifiable by the wake formations, including the 2S mode (two single vortices of opposite signs formed per oscillation cycle), P+S mode (one pair and one single vortex formed per cycle) and the 2P mode (two pairs of vortices formed per cycle). On the other hand, Leontini, Lo Jacono and Thompson [6] studied the flow around an in-line oscillatory cylinder, where vortex shedding synchronises with the forced oscillation at a rational ratio of $f_s/f_d = (N-1)/N$, where f_s is the adjusted vortex shedding frequency as a result of structural motion and N is an integer. Integer numbers as large as 8 were observed [6], i.e., the P8 mode. Most recently, Tang et al. [9] demonstrated that the mode ratio of f_s/f_d can be any fractional ratios p/q on the (A, f_d)-plane, where p and q are integers. It was also shown that the synchronised flow does prefer p/q composed by small integers over large ones, such as that the region occupied by mode 1/4 is much wider than that of 3/4. In addition, mode ratios with even denominator appear in a larger region than those with odd denominator, such that region of mode 2/3 takes less space than 3/4.

However, these works focused on one-direction translation motion. Less well understood is how the flow behaves around a cylinder due to a two-component oscillation in both the transverse and in-line directions (figure 1), in which case limited study has shown the wake does behave differently [7]. Two-component oscillations are frequently observed around offshore structures subject to coexisting non-collinear flows or two-degree-of-freedom vortex-induced vibration (VIV). This work is motivated by this knowledge gap among an abundance of published works on how the flow develops in the wake of an oscillatory cylinder. The Reynolds number (Re) based on the freestream velocity (U_∞) and diameter of the cylinder (D) was fixed at $U_\infty D/\nu = 100$, where ν is the viscosity of the fluid. The normalised amplitude ($A^* = A/D$) of the forced oscillation was chosen at 0.4. As illustrated in figure 1, three directions have been considered, which are $\alpha = 0°$ (in-line), 45° (inclined), and 90° (transverse). We report the wake flow features and hydrodynamic loading on the cylinder here. The variety of flow synchronisation modes, as discussed above, is shown to be enriched for the case of the inclined oscillation.

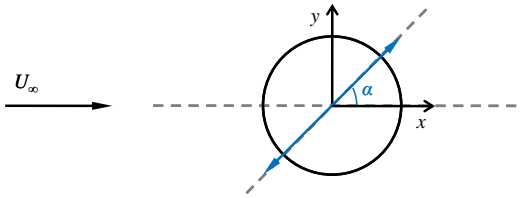

Figure 1: Illustration of the present study at $(Re, A^*) = (100, 0.4)$ and the coordinate definition. Three attacking angles between the sinusoidal oscillation direction and the uniform far-field flow have been considered, i.e., $\alpha = 0°$ (in-line), 45° (inclined), and 90° (transverse).

Sources	$\overline{C_D}$	C_{L-rms}	St
Present	1.345	0.232	0.165 97
Henderson (1995) [4]	1.35	-	-
Singh and Mittal (2005) [8]	1.35	0.25	0.166
Tong et al. (2014) [10]	1.37	0.23	0.172

Table 1: Comparison of the statistics related to a circular cylinder in steady flow at $Re = 100$.

Numerical method and model validation

The numerical study was carried out based on a two-dimensional (2-D) model. The governing equations for the flow are the incompressible Navier−Stokes (NS) equations. Direct numerical simulations are carried out using an open-source spectral/hp element code, Nektar++ [2]. The code employs high-order quadrilateral expansions within each element using the modified Legendre basis. A second-order implicit-explicit time-integration scheme is chosen from the embedded NS solver, along with the velocity correction splitting scheme and a continuous Galerkin projection. The harmonic cylinder oscillation is implemented

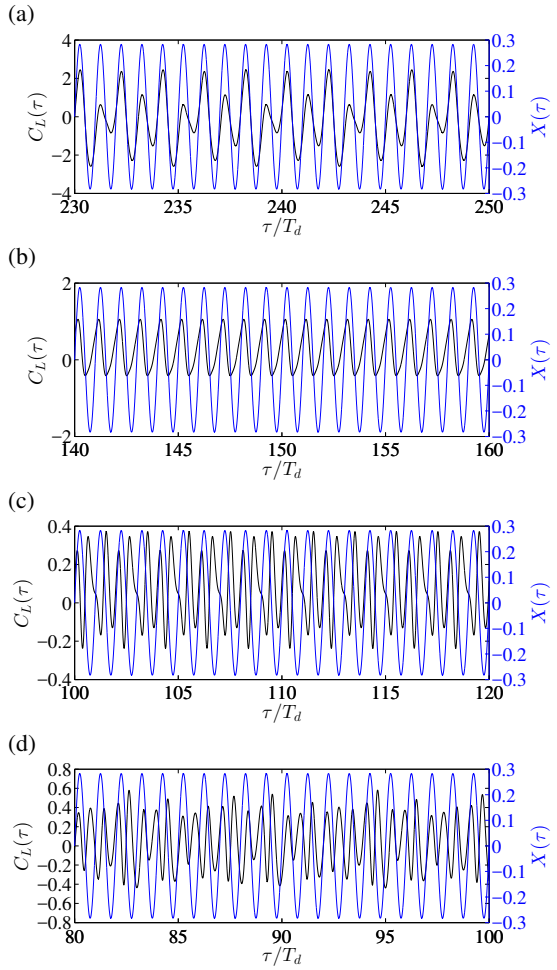

Figure 2: Time history of lift coefficient (black lines) at $\alpha = 45^\circ$ and (a) λ^*= 4; (b) λ^* = 6, (c) λ^* = 8 and (d) λ^* = 10, along with the position of the cylinder in the x-direction (blue lines).

through a moving frame fixed on the cylinder and the mesh used is similar to that reported in Tang et al. [9]. A validation check was carried out for flow around a stationary cylinder, as detailed in Table 1. The numerical results on $\overline{C_D} = \overline{F_x/(\rho U_\infty^2 D)}$, $C_{L-rms} = rms[F_y/(\rho U_\infty^2 D)]$ and St compared well with published data, which are the mean drag coefficient, root-mean-square (rms) of lift coefficient and the Strouhal number ($St = f_{St}D/U_\infty$). Here, the vortex shedding frequency for the stationary cylinder, f_{St}, is obtained by carrying out a Fast Fourier Transform (FFT) on C_L.

Result Discussions

For all three attacking angles, a range of oscillation frequencies were investigated, which is presented as $\lambda^* \equiv U_\infty/(f_d D)$, similar to the definition of reduced velocity (U_r) in VIV. The value of λ^* represents the distance that freestream travels in one cycle of cylinder oscillation, which was referred to as wavelength [11]. Specifically, $\lambda^* \in [2, 16]$ with an increment of 0.2 was studied, in the aim to cover the range of U_r in VIV with relatively large amplitude responses.

Synchronisation modes identification

Firstly, we present the time traces of lift coefficient and their comparison with the $x-$direction displacement of the cylinder, $X(\tau)$, in figure 2. The instantaneous flow fields for the corresponding cases are given in figure 3, to illustrate the variety

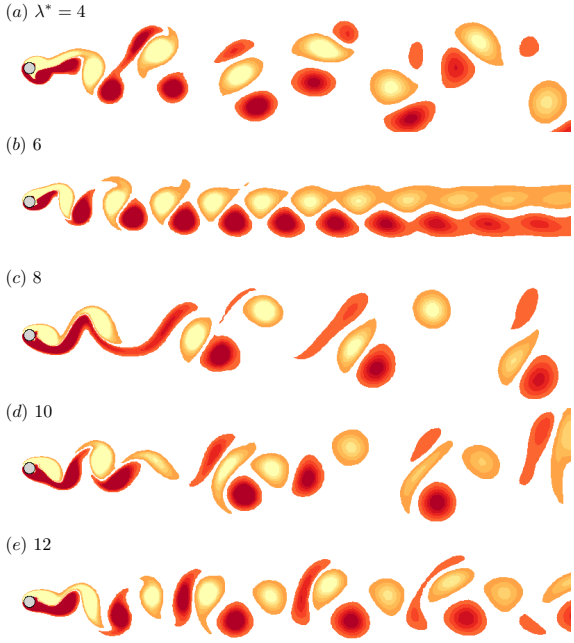

Figure 3: Comparison of the instantaneous flow fields as represented by the vorticity ($\omega_z = \bigtriangledown \times \mathbf{U}$) at $\alpha = 45^\circ$, with all zones of synchronisation as given in figure 5. (a) λ^* = 4 (zone ①), (b) λ^* = 6 (zone ②), (c) λ^* = 8 (zone ③), (d) λ^* = 10 (non-synchronisation) and (e) λ^* = 12 (zone ④).

of flow synchronisation modes at $\alpha = 45^\circ$. Here, $T_d = 1/f_d$ and the time scale τ is non-dimentionalised by D/U.

For $\lambda^* = 4 \sim 8$, the hydrodynamic forces and cylinder motion display three different synchronisation features. (i) At $\lambda^* = 4$, $C_L(\tau)$ oscillates four times in four cycles of oscillation, but has different-sized peaks in each of these four cycles, despite having the same frequency as the cylinder oscillation. (ii) These peaks in $C_L(\tau)$ change to be the same at $\lambda^* = 6$, where there appears to be a phase difference between the two signals, but they perfectly synchornise to each other. The former is a 4/4 mode while the later is a 1/1 mode, based on to the classification approach in Tang et al.[9]. (iii) When it moves to $\lambda^* = 8$, $C_L(\tau)$ oscillates 3 times in two cycles of displacement, giving rise to a 3/2 mode. The last panel at $\lambda^* = 10$ shows a non-synchornised case, where $C_L(\tau)$ shows no trend of repeating in the time window, and in fact $C_L(\tau)$ never precisely repeats itself for a tremendous amount of time in the simulation. Therefore, for the above cases, $C_L(\tau)$ shows the same dominating frequency as the displacement in cases of figure 2 (a) and (b), but has a frequency of 1.5 times f_d at (c).

Affected by displacement-induced inertia force, the amplitude of the lift coefficient can be relatively large (figure 2a). In addition, figure 2 (a) and (c) also show that C_L-amplitude can vary greatly from cycle to cycle of vortex shedding and this is thought to be related to active adjustment of vortex formation and shedding as the cylinder moves. It is seen that for $\lambda^* = 4$, $C_L(\tau)$ oscillates roughly around the zero-mean value, but at a non-zero-mean value for $\lambda^* = 6$, which corresponds to different wake formations, as given in figure 3 (a) and (b). The non-zero-mean $C_L(\tau)$ is apparently induced by the inclined wake formation at $\lambda^* = 6$, where the wake leans to $y-$direction and thus $\overline{C_L(\tau)}$ is larger than 0. At $\lambda^* = 4$ in figure 3 (a), the vortices form a group of 3 (P+S) and convect downstream in a staggered manner. The P-vortices are much larger than the

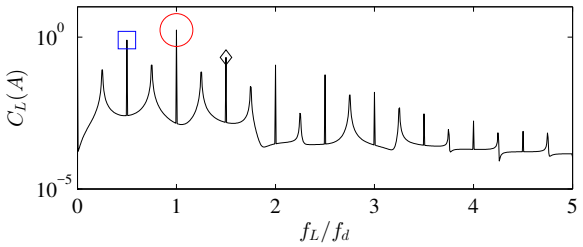

Figure 4: Illustration on the multiple peaks in Fast Fourier Transform (FFT) of the lift coefficient of an oscillatory cylinder in steady flow at $(\lambda^*, \alpha) = (4, 45°)$. The maximum three peaks are sequentially indicated by ◯, □ and ◊ with sizes correlating to the magnitudes.

S-vortex, and this is the reason for the different-sized peaks in figure 2 (*a*). At $\lambda^* = 8$ in figure 3 (*c*), the vortices form a group of 4 (2P) and the four vortices are again not uniform in size. Figure 3 gives five distinctive flow fields, representing the zones that will be shown later in figure 5. For these relatively simple cases of synchronisation, the wake is comparable to the 2S (*b*), P+S (*a*) and 2P (*c*) modes as discussed earlier, but the wake formation can be so rich that the classification based on $f_L/f_d = p/q$ modes [9] shall be used for the inclined cylinder oscillation.

Flow synchronisation

The flow synchronisation is investigated by analysing the phase diagram of forces, as well as the frequency component of the lift coefficient, as given in figure 4. A synchronised case is characterised by multiple but repeatable peaks over $f_L/f_d \in (0,1),(1,2)\cdots$. In particular for this case, the largest peak is found at $f_L/f_d = 1$, attributing to the external perturbation, while the second largest is at 0.5, which is due to vortex shedding. The peak at 0.25 is related to the change in force magnitude from every second cycle, as seen in figure 2. All the other peaks are just the combination of these three peaks, or the super-harmonic of 1/4 in figure 4 for modes 4/4. This is because in the synchronised case, the ratio of f_L/f_d is a rational ratio p/q, and all peaks are just N/q.

Figure 5 picks the leading three peaks as illustrated in figure 4 and compares these peaks at three angles of attack. It reveals information related to the flow field, including the relative energy of the peaks, the frequency of vortex shedding, the peak locations as a function of λ^*, as well as zones of synchronisation of the flow field with cylinder oscillation at different attacking angles and λ^*. The frequency ratio of f_L/f_d does not change with varying λ^* in the zone of synchronisation. For the peaks, the zero attack in figure 5(*a*) sees no leading peaks located at $f_L/f_d = 1$ at small λ^* (<5), which is because the in-line oscillation minimises the effect of cylinder motion to vortex formation as compared to $\alpha = 45°$ and 90° at similar λ^*. The flow synchronization at low λ^* at α =0° occurs in a manner that a pair of vortices shed in every two cycles of oscillation, thus $f_s/f_d = 1/2$. This similar mode is observed but in an adjusted form at $\alpha = 45°$, such as in the modes of 4/4, and totally disappears at $\alpha = 90°$. In general, a more rich range of peaks appears at $\alpha = 0°$ and 45° than that at 90°, possibly due to the transverse oscillation inducing a more direct impact on the vortex formation at the two shear layers around the cylinder.

For flow synchronisation, $\alpha = 45°$ experiences four distinct ranges of synchronisation, where respectively, the vortex shedding frequency locks to $0.5f_d$, f_d, $1.5f_d$ and $2f_d$. With the change of α, only the first three are seen at $\alpha = 0°$ and only

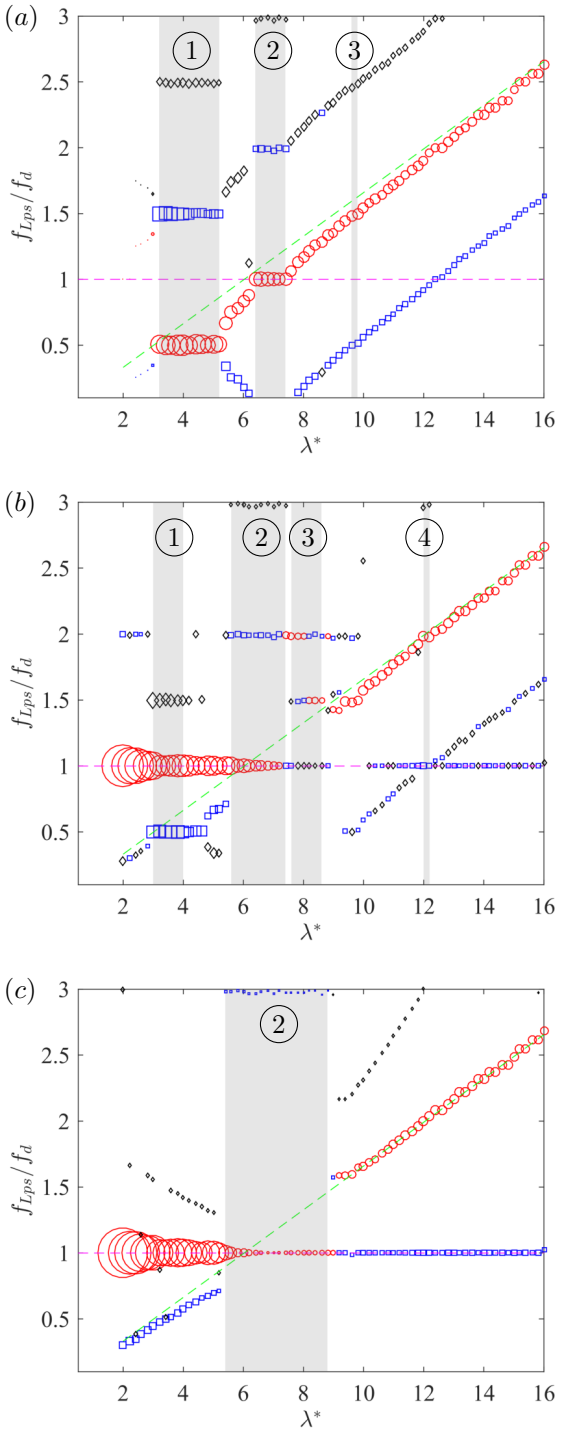

Figure 5: Comparison on the three leading peaks (f_{Lps}) in FFT of the lift coefficient as a function of λ^* at (*a*) $\alpha = 0°$ (in-line), (*b*) 45° (inclined) and (*c*) 90° (transverse). The circled numbers indicate the zone of synchronisation, where ①, ②, ③ and ④, respectively, show zone of wake synchronisation to $0.5f_d$, f_d, $1.5f_d$ and $2f_d$. The purple-dashed horizontal line is the driving frequency of cylinder oscillation, which dominated the peaks at low λ^* (except $\alpha = 0°$). The green-dashed diagonal line represents the natural vortex shedding frequency without cylinder oscillation ($= f_{St}/f_d$), which dominates the peak at large λ^*. The primary synchronisation zone is zone ① at $\alpha = 0°$, but zone ② at $\alpha = 90°$. The way these peaks were selected is demonstrated in figure 4 and the sizes are scaled for all angles.

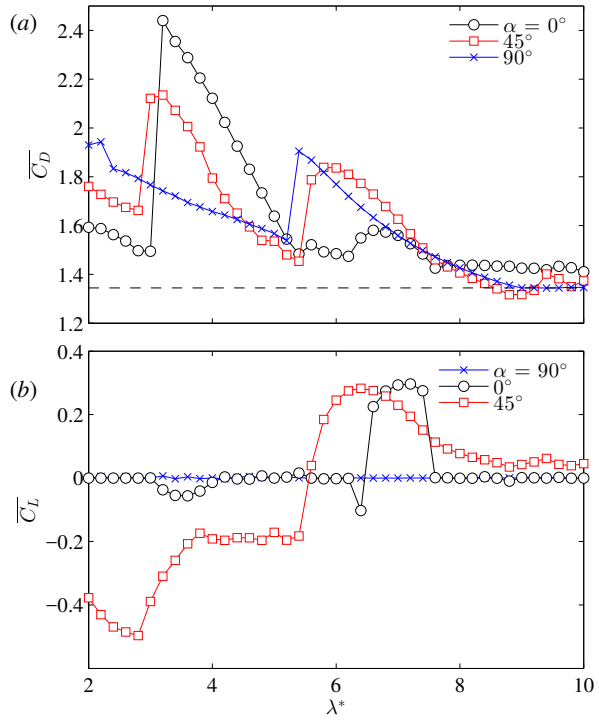

Figure 6: Comparison of the mean drag and lift coefficients as a function of λ^* at three attacking angles at $(Re, A^*) = (100, 0.4)$. $\overline{C_D}$ for the non-oscillatory cylinder in otherwise the same flow condition is given as a dashed line, while $\overline{C_L}$ for the stationary cylinder is 0.

one at $\alpha = 90°$ (to f_d). This feature indicates that by allowing vibrations in both transverse and in-line directions, the wake may show more types of synchronised flows. Another notable feature is the size of the peaks at the primary synchronisation zone to f_d (zone ②), where circles at $\alpha = 90°$ appear to be much smaller than those at 0° and 45°, which is noteworthy considering the inertia force induced by cylinder displacement at 90° should be the largest among the three (which is indeed the case at $\lambda^* = 2$). By comparison, circles appear to be much larger at $\alpha = 0°$ in zone ②. For non-synchronised cases, figure 5 shows a much richer range of peaks at $\alpha = 0°$ and 45° than that at 90°. With λ^* increasing to 10 and beyond, only very few cases can be classified as synchronisation.

The angles of attack and the types of synchronisation affect the force statistics greatly, as demonstrated in figure 6. For most of the cases at $\alpha = 45°$, $\overline{C_L}$ is non-zero, as compared to that of mostly zero for the transverse-oscillation condition. In agreement with published study [9], $\overline{C_L}$ can be non-zero for the in-line oscillation condition, but the inclined oscillation enhances the wake inclination to an extent that the magnitude of $\overline{C_L}$ can be larger than 0.5 at certain λ^* (such as at around $\lambda^* = 3$). $\overline{C_D}$ (which is not affected by inertia force at $\alpha = 90°$) also shows ups and downs with varying λ^* at all angles of attack and in particular, $\overline{C_D}$ also varies greatly with α. For instance, the largest $\overline{C_D}$ is found at $\alpha = 90°$ for $\lambda^* = 2.0 \sim 3.0$, at $\alpha = 0°$ for $\lambda^* = 3.4 \sim 5.0$, and at $\alpha = 45°$ for $\lambda^* = 6.0 \sim 7.2$. The variety in changes in the loading are related to the synchronisation between wake flows and cylinder oscillation. This is because as the separated flow becomes resonant, it is associated with the coalescence of small vortices and thus a more organised wake flow, which leads to an enhanced shear layer and a stronger entrainment wake [12]. Therefore, flow synchronisation generally induces relatively large forces.

Conclusions

The flow around a circular cylinder undergoing controlled oscillation in a steady current at three angles of attack has been studied. It shows that the inclined oscillation, where the motion intersect the freestream at a 45°, leads to substantial changes to the force features from those of the in-line (0°) or transverse (90°) oscillations. These changes are shown to be related to the flow synchronisation phenomenon between vortex shedding and the cylinder motion, which is found in a wider range of oscillation frequencies for the inclined oscillation.

Acknowledgements

This work was supported by resources provided by the Pawsey Supercomputing Centre.

References

[1] Bishop, R. and Hassan, A. (1964). The lift and drag forces on a circular cylinder oscillating in a flowing fluid, Proc. R. Soc. A, 277, 51–75.

[2] Cantwell, C., Moxey, D., Comerford, A., Bolis, A., Rocco, G., Mengaldo, G., De Grazia, D., Yakovlev, S., Lombard, J.-E. and Ekelschot, D. (2015). Nektar++: An open-source spectral/hp element framework, Comput. Phys. Commun., 192, 205–219.

[3] Carberry, J., Sheridan, J. and Rockwell, D. (2005). Controlled oscillations of a cylinder: forces and wake modes, J. Fluid Mech., 538, 31–69.

[4] Henderson, R. D. (1995). Details of the drag curve near the onset of vortex shedding, Phys. Fluids, 7, 2102–2104.

[5] Konstantinidis, E. and Balabani, S. (2007). Symmetric vortex shedding in the near wake of a circular cylinder due to streamwise perturbations, J. Fluids Struct., 23, 1047–1063.

[6] Leontini, J. S., Lo Jacono, D. and Thompson, M. C. (2013). Wake states and frequency selection of a streamwise oscillating cylinder, J. Fluid Mech., 730, 162–192.

[7] Ongoren, A. Rockwell, D. (1988). Flow structure from an oscillating cylinder Part 1. Mechanisms of phase shift and recovery in the near wake, J. Fluid Mech., 191, 197–223.

[8] Singh, S. and Mittal, S. (2005). Vortex-induced oscillations at low Reynolds numbers: hysteresis and vortex-shedding modes, J. Fluids Struct., 20, 1085–1104.

[9] Tang, G., Cheng, L., Tong, F., Lu, L. and Zhao, M. (2017). Modes of synchronisation in the wake of a streamwise oscillatory cylinder, J. Fluid Mech., 832, 146–169.

[10] Tong, F., Cheng, L., Zhao, M., Zhou, T. and Chen, X.-B. (2014). The vortex shedding around four circular cylinders in an in-line square configuration, Phys. Fluids, 26, 024112.

[11] Williamson, C. and Roshko, A. (1988). Vortex formation in the wake of an oscillating cylinder, J. Fluids Struct., 2, 355–381.

[12] Wu, J.-Z., Lu, X.-Y., Denny, A. G., Fan, M. and Wu, J.-M. (1998). Post-stall flow control on an airfoil by local unsteady forcing, J. Fluid Mech., 371, 21–58.